Electronic Supplementary Material (ESI) for Catalysis Science & Technology.

SUPPORTING INFORMATION

Supported Rh_2O_3 sub-nanometer size particles for direct amination of ethylene with piperidine

Manideepa Sengupta,[a, b] Tuhin Suvra Khan,[a] Subhasis Das,[c] Gurmeet Singh,[a] Ravi Kumar,[d] Dibyendu Bhattacharya,[d] M. Ali Haider,[e] Sk Manirul Islam,*[b] and Ankur Bordoloi*[a]

[a] Nano Catalysis, Light Stock Processing Division
CSIR-Indian Institute of Petroleum
Dehradun-248005, Uttarakhand (India).
E-mail: ankurb@iip.res.in

[b] Department of Chemistry
University of Kalyani
Kalyani-741235, West Bengal (India).

[c] Ruhr-University Bochum, Chemistry and Biochemistry
Universitätsstr. 150, 44801 Bochum (Germany).

[d] Atomic & Molecular Physics Division,
Bhabha Atomic Research Centre, Mumbai 400085 (India).

[e] Department of Chemical Engineering, IIT Delhi (India).

Corresponding author:

Dr. Ankur Bordoloi, **E-mail**: ankurb@iip.res.in

Prof. Sk Manirul Islam, **Email:** manir65@rediffmail.com

Experimental Section

General Considerations

1.1. Catalyst Characterization

All chemicals and solvents obtained from Sigma-Aldrich Co. and were used without any further purification. Transmission Electron Microscopy (TEM) images were recorded on a JEM 2100 (JEOL, Japan) microscope, and samples were prepared by mounting an ethanol-dispersed sample on a lacey carbon formvar coated Cu-grid. Elemental mapping was collected with the same spectrophotometer. X-ray photoelectron spectroscopy (XPS) was performed with a Thermo Scientific K-Alpha XPS instrument and binding energies (±0.1 eV) were determined with respect to the C1s peak at 284.58 eV. Percentage of Rh loading in Rh/SiO_2 was confirmed by inductively coupled plasma atomic emission spectroscopy (ICP-AES) using PS 3000 UV (DRE), Leeman Labs Inc. (USA). Fourier transform infra-red (FT-IR) spectra were recorded on a Thermo Nicolet 8700 (USA) instrument with the operating conditions: resolution: 4 cm^{-1}, scan: 36, operating temperature: 23–25°C and the frequency range: 4000-500 cm^{-1}. Spectra in the lattice vibrations range were recorded for wafers of sample mixed with KBr. The powder X-ray diffraction (XRD) patterns were recorded on a Proto Advance X-ray diffractometer fitted with a Lynx eye high-speed strip detector using Cu $K\alpha$ radiation.

Extended X-ray Absorption Fine Structure (EXAFS) measurements have been carried out to probe the local structure around the Rh atom of the RSSR, RSS, RSF and Rh_2O_3 samples at Rh K-edge. The XAS measurements have been carried out at the Energy-Scanning EXAFS beamline (BL-9) at the Indus-2 Synchrotron Source (2.5 GeV, 100 mA) at Raja Ramanna Centre for Advanced Technology (RRCAT), Indore, India.[1] This beamline operates in the energy range of 4 KeV to 25 KeV. The beamline optics consists of a Rh/Pt coated collimating meridional cylindrical mirror and the collimated beam reflected by the mirror is monochromatized by a Si (111) (2d=6.2709 Å) based double crystal monochromator (DCM).

The second crystal of DCM is a sagittal cylinder used for horizontal focusing while a Rh/Pt coated bendable post mirror facing down is used for vertical focusing of the beam at the sample position. Rejection of the higher harmonics content in the X-ray beam is performed by detuning the second crystal of DCM. In the present case, XAS measurements have been performed in transmission mode. For the transmission mode measurement, three ionization chambers (300 mm length each) have been used for data collection, one ionization chamber for measuring incident flux (I0), second one for measuring transmitted flux (It) and the third ionization chamber for measuring XAS spectrum of a reference metal foil for energy calibration. Appropriate gas pressure and gas mixtures have been chosen to achieve 10-20 % absorption in first ionization chamber and 70-90 % absorption in second ionization chamber to improve the signal to noise ratio. The absorption coefficient μ is obtained using the relation:

$$I_T = I_0 e^{-\mu x} \tag{1}$$

where, *x* is the thickness of the absorber.

To obtain the qualitative information about the local structure, oscillations in the absorption spectra $\mu(E)$ has been converted to absorption function $\chi(E)$ defined as follows:

$$\chi(E) = \frac{\mu(E) - \mu_0(E)}{\Delta\mu_0(E_0)} \tag{2}$$

Where, E_0 is absorption edge energy, $\mu_0(E_0)$ is the bare atom background and $\Delta\mu_0(E_0)$ is the step in $\mu(E)$ value at the absorption edge. The energy dependent absorption coefficient $\chi(E)$ has been converted to the wave number dependent absorption coefficient $\chi(k)$ using the relation,

$$K = \sqrt{\frac{2m(E - E_0)}{\mathrm{h}^2}} \tag{3}$$

where, m is the electron mass. $\chi(k)$ is weighted by k^2 to amplify the oscillation at high k and the $\chi(k)k^2$ functions are fourier transformed in R space to generate the $\chi(R)$ versus R spectra in terms of the real distances from the center of the absorbing atom. The set of EXAFS data analysis programme available within Demeter[2] software package have been used for EXAFS data analysis. This includes background reduction and Fourier transform to derive the $\chi(R)$ versus R spectra from the absorption spectra (using ATHENA[2] software), generation of the theoretical EXAFS spectra starting from an assumed crystallographic structure and finally fitting of experimental data with the theoretical spectra using ARTEMIS[2] software. The normalized XAS spectra of all samples are shown in figure 1. The $\chi(R)$ versus R plots at Rh K-edge were generated by fourier transform of $k^2\chi(K)$ vs. k spectra (figure 2) following the methodology described above over k range of 3.0-10.0 $Å^{-1}$ and are shown in figure 3. The data has been fitted in the range 1.0-3.0 Å in R space. The guess parameters and scattering paths have been generated assuming Rh_2O_3 crystal structure of all the samples. In the fitting process the co-ordination number (C.N), atom to atom bond distance (R) between the respective atomic pairs and the disorder factor (Debye –Waller factor) (σ^2), which gives the mean square fluctuation in the atomic bond lengths and the thermal disorder in the system, have been used as fitting parameters and the best fit parameters have been shown in Table 1. The goodness of fit has been determined by the value of the R_{factor} defined by:

$$R_{factor} = \sum \frac{[\mathrm{Im}(\chi_{dat}(r_i) - \chi_{th}(r_i)]^2 + [\mathrm{Re}(\chi_{dat}(r_i) - \chi_{th}(r_i)]^2}{[\mathrm{Im}(\chi_{dat}(r_i)]^2 + [\mathrm{Re}(\chi_{dat}(r_i)]^2} \qquad (4)$$

where, χ_{dat} and χ_{th} refer to the experimental and theoretical $\chi(r)$ values respectively and Im and Re refer to the imaginary and real parts of the respective quantities.

1.2. Catalyst Synthesis

All the chemicals and solvents have been purchased from Merck and used without any further purification.

1.2.1. Synthesis of mesoporous Silica:

In a typical synthesis, 1 g of triblock copolymer P123 (EO20PO70EO20) was dissolved in 15 g of double distilled water. To this solution, 30 g of 2 M hydrochloric acid solution was added and stirred overnight at 35 ℃. After P123 get fully dissolved, 3 mL of 1 wt.% PVA solution was added followed by dropwise addition of 2.1 g tetraethoxysilane. The resultant solution was kept under constant stirring for 24 h. After this, the solution was transferred to a Teflon-lined autoclave, and aged at 100 ℃ for another 24 h. Finally, the mixture was filtered, dried at 100 ℃ and calcined at 500 ℃ for 4h.

1.2.2. Fabrication of Rh_2O_3 sub nanoparticles within mesoporous Silica:

Rhodium oxide subnanoparticles have been embedded within mesochannels of silica via organic matrix deposition method. In a typical synthetic procedure, 0.5 g of mesoporous silica was added in 500 mL double distilled water under stirring. Next, after well mixing, an aqueous solution of Rhodium (II) acetate dimer was added dropwise to the mixture under sonication and after complete dissolution of rhodium salt, urea [$Rh/(NH_2)_2CO$ =1:5 mole ratio] was further added and the mixture was slowly heated and refluxed at 90 C under stirring for 48 h. The resultant mixture of $Rh(OH)_3/SiO_2$ was then cooled, filtered, washed several times with aqueous alcholic solution, and dried at 100 C. Finally, Rh_2O_3 subnanoparticles incorporated mesoporous SiO_2 was obtained after treating $Rh(OH)_3/SiO_2$ under flow of air at 550 C for 4 h with constant heating rate of 1 C/ min. A scheme for the synthesis of SiO_2 supported Rh_2O_3 sub nanoparticles has been represented on figure S1.

1.3. SiO_2 supported Rh_2O_3 sub nanoparticles catalysed hydroamination of ethylene with piperidine

Catalytic activity was tested in a 50 mL Parr reactor. In a typical experiment, the 50 mL stainless steel reactor was charged with 0.0294 mol piperidine and Rh/SiO_2-fresh catalyst (30 mg, 8.163×10^{-3} mmol of Rh) and bath-sonicated for 2 mins for efficient dispersion of the catalyst. Then the reactor was fixed and after removing existing air via vacuum pump, flushed with ethylene gas two times to ensure complete evacuation of air within the reactor. Finally, the reactor was charged with 12 Bar ethylene gas. The reactor containing resulting mixture was then heated slowly to 180 C and kept over a period of 24 h under stirring. At the end of the reaction, the reactor was cooled and catalyst was separated by filtration and the product was analysed and piperidine conversion was obtained by gas chromatograph (GC, Agilent 7890) with an HP5 capillary column (30 m length, 0.28 mm id, 0.5 mm film thickness) and flame ionization detector (FID). The product identification was performed from GC-MS. The filtered catalyst Rh/SiO_2-spent was washed several times with ethanol and double distilled water and regenerated by calcining under air flow at 550 C for 4h. A scheme of the reactor set up has been presented on fig S2.

1.4. Catalyst recyclability

To verify the stability of Rh/SiO_2 catalyst, recycle test up to 4 runs have been performed and represented on fig S7. The fresh catalyst gave 18.3 % conversion of piperidine. For the recyclability test, the catalyst was separated washed and after calcining at 550 C under air flow, the regenerated Rh/SiO_2 catalyst was used with a fresh reaction mixture in the second run and the procedure was repeated for the next three runs. The results showed that the conversion of phenylacetylene was decreased to 16 % in the second run and after which minute decrease (1~2 %) was noticed, might be due to handling loss with constant selectivity (>82 %) for the rest of the runs.

DFT Method:

For the hydroamination reaction between piperidine and ethylene over silica supported Rh_2O_3 sub nanoparticles, DFT calculations were performed using the periodic plane-wave Vienna *ab initio* Simulation Package (VASP 5.3.5).[3] Two different Rh_2O_3 catalyst models were used in this study. The small highly dispersed Rh_2O_3 nanoparticles were represented by a spherical Rh_2O_3 nanocluster of diameter 1.6 nm, having chemical formula $Rh_{80}O_{120}$. Materials Studio GUI was used to obtain the $Rh_{80}O_{120}$ cluster. The Rh_2O_3 crystal was obtained from the Materials Design database (ID: mp-1716), [The Materials Project. Materials Data on Rh_2O_3 by Materials Project. United States: N. p., 2020. Web. doi:10.17188/1192363]. The build nanostructure tool in materials studio was then employed to cut a sphere shape cluster of size 1.6 nm (in diameter) from the bulk Rh_2O_3.

The $Rh_{80}O_{120}$ nanocluster was kept in a periodic box of size 30Å x 30Å x 30Å (Figure S8a). The bigger agglomerated nanoparticles were represented using a Rh_2O_3(100) surface slab. The Rh_2O_3(100) surface was modelled using four-layer slab. A 6 x 6 supercell, having a vacuum of 20 Å along the z-axis was used for the DFT calculation of Rh_2O_3(100) surface (Figure S8b). The Rh_2O_3(100) surface was found to be most stable Rh_2O_3 surface as can be seen in the relative surface stability energies given in Table S1.

Table S1. Relative stability of Rh_2O_3 surfaces.

Surface	Relative stability per Rh_2O_3 unit (eV)
(100)	0.00
(001)	0.85
(010)	0.80
(110)	0.50
(111)	0.81

The DFT calculations over the $Rh_{80}O_{120}$ nanocluster and $Rh_2O_3(100)$ surface were performed using Revised Perdew-Burke-Erbzerhof (RPBE) GGA exchange-correlation functional,[4] along with the Vanderbilt ultra-soft pseudopotentials.[5] Plane wave basis energy cut-off of 396 eV was used. The van der Walls dispersion corrections were incorporated using the Grimme DFT-D3 correction with Becke-Jonson damping.[6] The surface Brillouin zone is sampled using a 2 x 3 x 1 Monkhorst–Pack grid.[7] An energy and force convergence criteria have been set to $1x10^{-6}$ eV and 0.05 eV/Å, respectively, used for the geometry optimizations.

The adsorption energy (E_{ads}) of the surface intermediates were calculated as follows:

$$E_{ads} = E_{surf+adsorbate} - (E_{surf} + E_{adsorbate,gas}) \quad (1)$$

where E_{surf}, $E_{surf+adsorbate}$, and $E_{adsorbate,\ gas}$ denotes the energy of the clean surface, energy of adsorbate species at the surface and energy of adsorbate in gas-phase, respectively.

The reaction energy (E_{rxn}) of the elementary surface reaction steps is evaluated as the difference between final (product) and initial state (reactant) energies, as per the equation:

$$E_{rxn} = E_{final} - E_{initial} \quad (2)$$

where $E_{initial}$ and E_{final} is the energy of the initial and final state of the elementary surface reaction step, respectively.

Nudged Elastic Band (NEB) method as proposed by Henkelman et al.[8] was used to obtain the transition state energies and geometries. In the NEB method the minimum energy path joining the reactant and the product is constructed with of 8 images between the initial and final states. The energy and force convergence criteria $1x10^{-4}$ eV and 0.1 eV/Å, respectively were used for the NEB calculations. Geometries of the transition state were determined using the climbing image NEB method.[9] Activation barrier of the elementary reaction step is evaluated as the difference between the transition state and the reactant state, given by:

$$E_a = E_{TS} - E_{reactant} \quad (3)$$

where E_{TS} and $E_{reactant}$ represents the energy of the transition state and reactant of the elementary step, respectively.

For both the geometry optimizations and NEB calculations, the two bottom layers of the $Rh_2O_3(100)$ surface slab were fixed at their bulk positions, where the top two layers along with the adsorbates were allowed to relax.

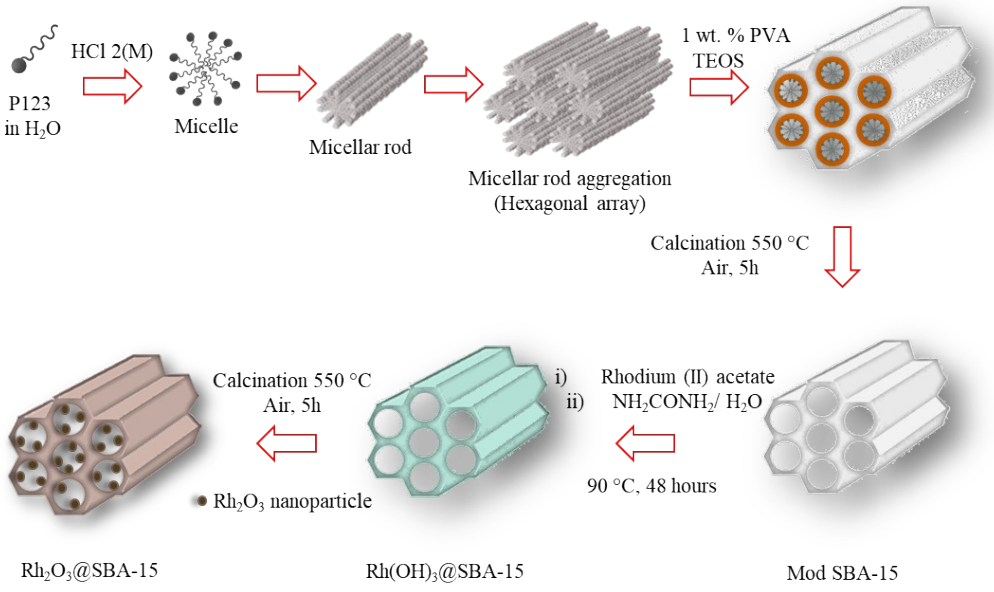

Figure S1. Schematic representation for synthesis of SiO_2 supported Rh_2O_3 sub nanoparticles

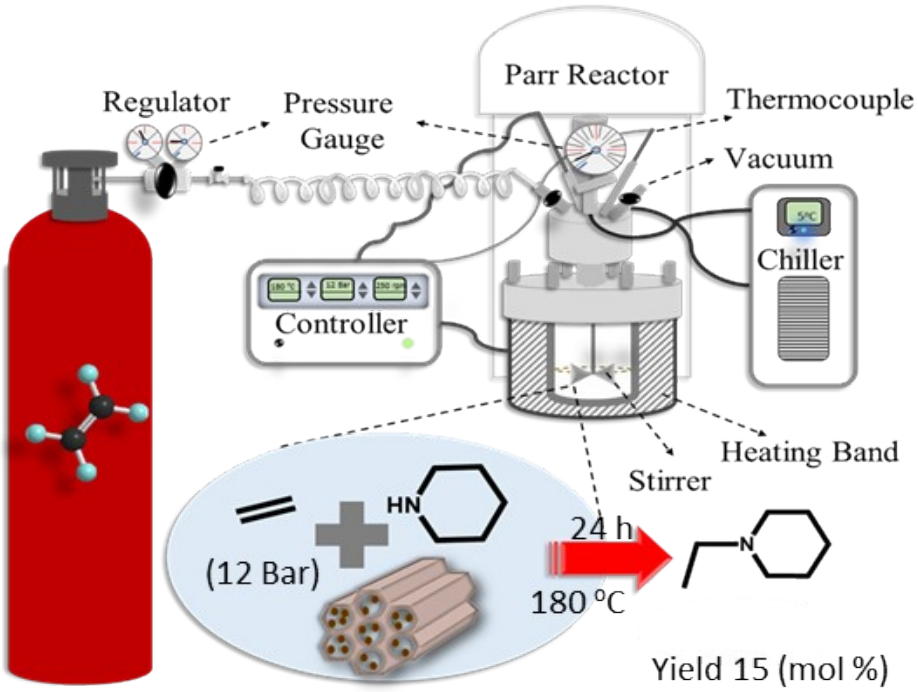

Figure S2. Schematic presentation of reactor set up for direct addition of piperidine to ethylene with SiO_2 supported Rh_2O_3 sub nanoparticles

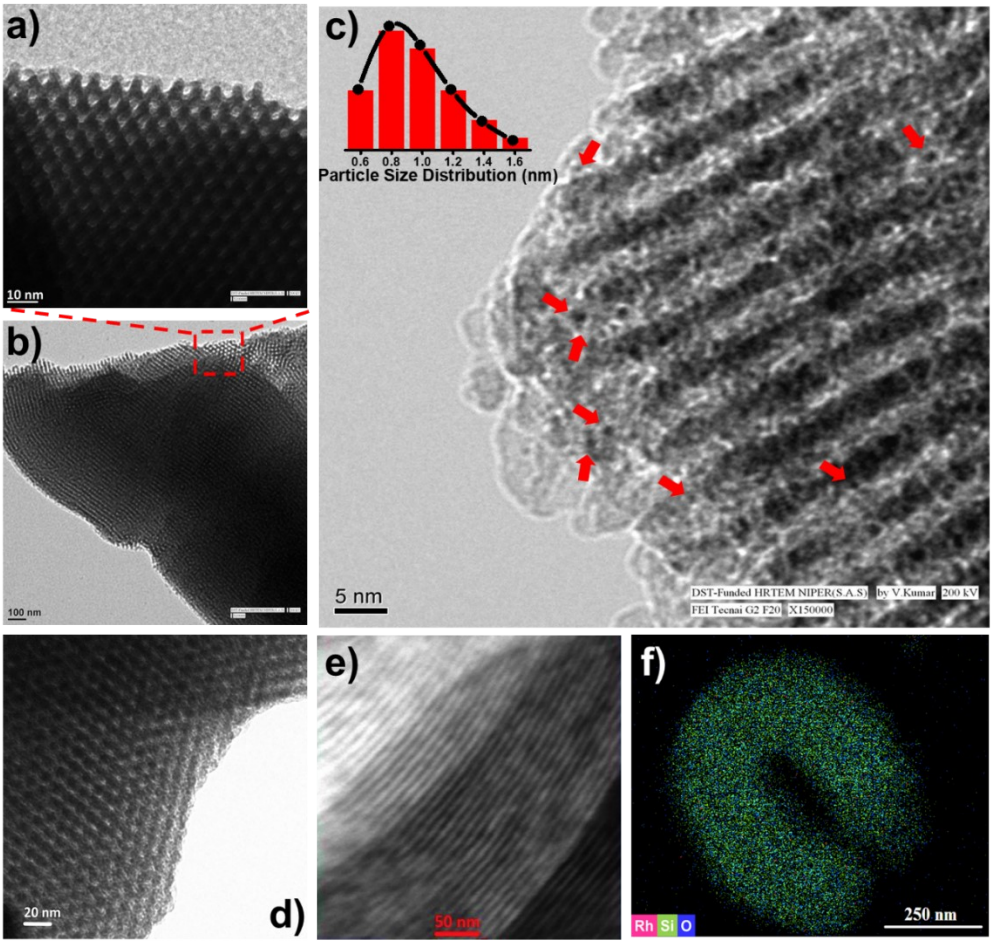

Figure S3. HRTEM images of a, b) mesoporous silica, c, d) Rh/SiO_2-spent catalyst (inset showing particle distibution histogram), e) HAADF STEM image, and f) elemental mapping for Rh/SiO_2-fresh catalyst.

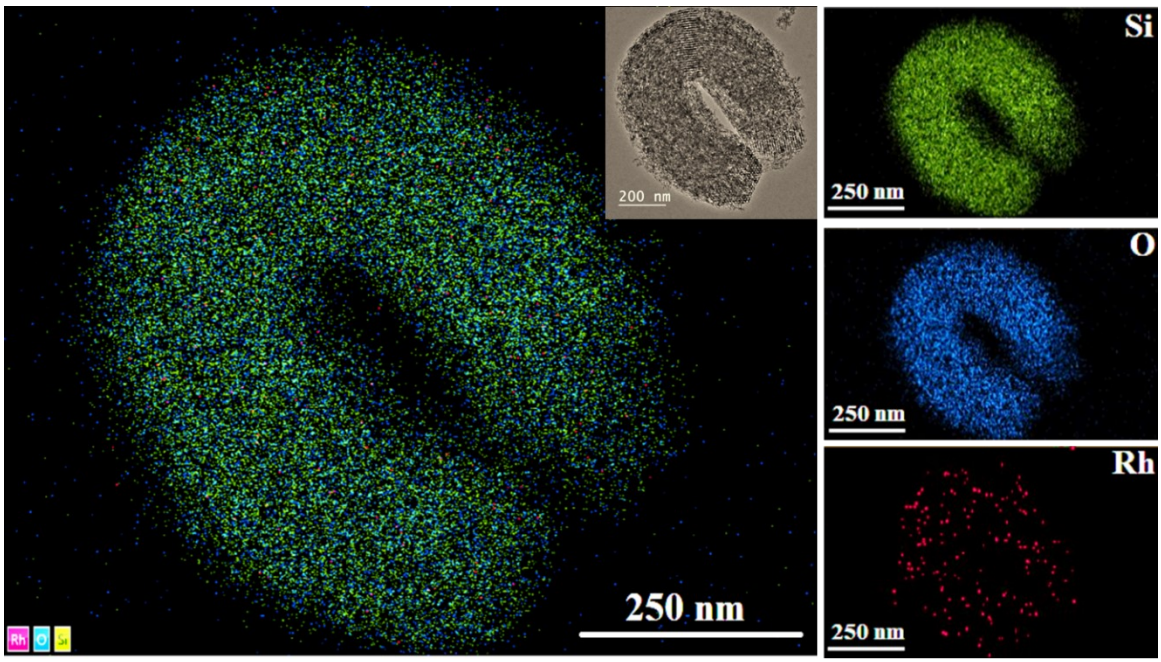

Figure S4. Elemental Mapping of Rh/SiO_2-fresh catalyst.

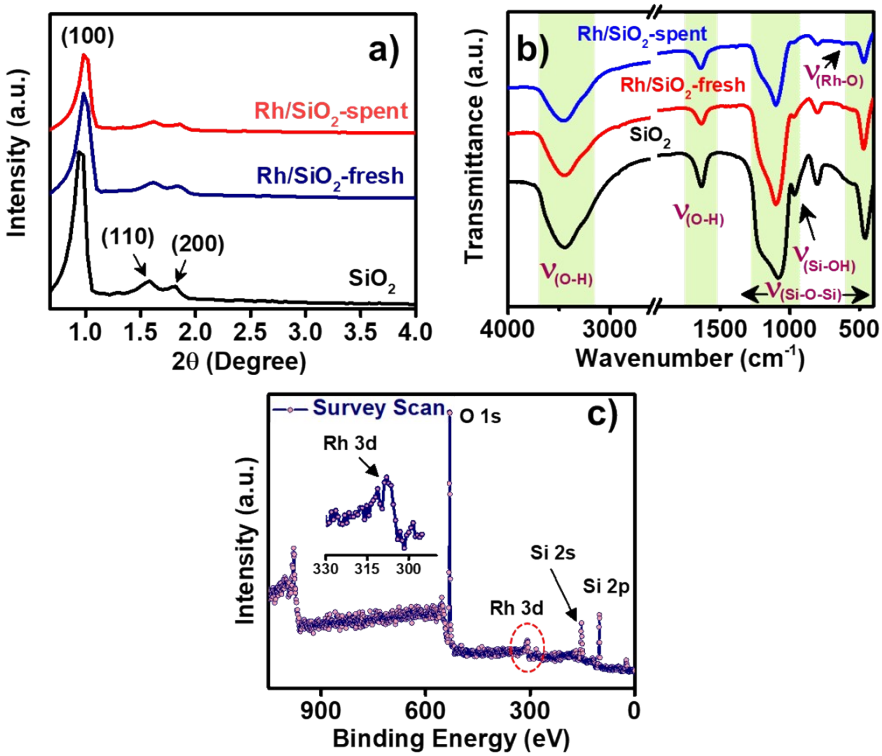

Figure S5. a) Low angle XRD pattern and b) FT-IR specta of SiO_2 and Rh/SiO_2 catalysts, c) Survey scan of Rh/SiO_2-fresh catalyst.

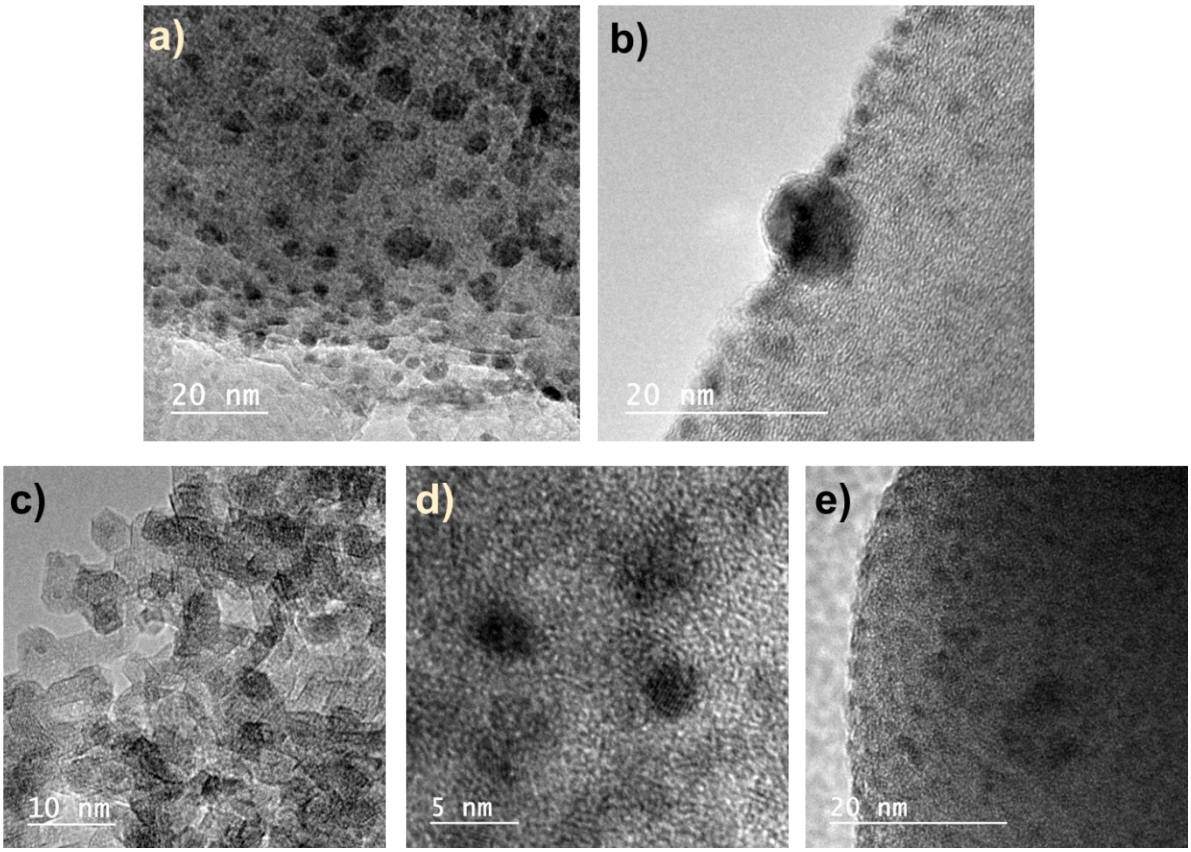

Figure S6. HRTEM images of a) Rh/Hydrotalacite, b) Rh/Carbon nanotubes, c) Rh/Al_2O_3, d) Rh/Acitivated Carbon, e) Rh/ZSM-5

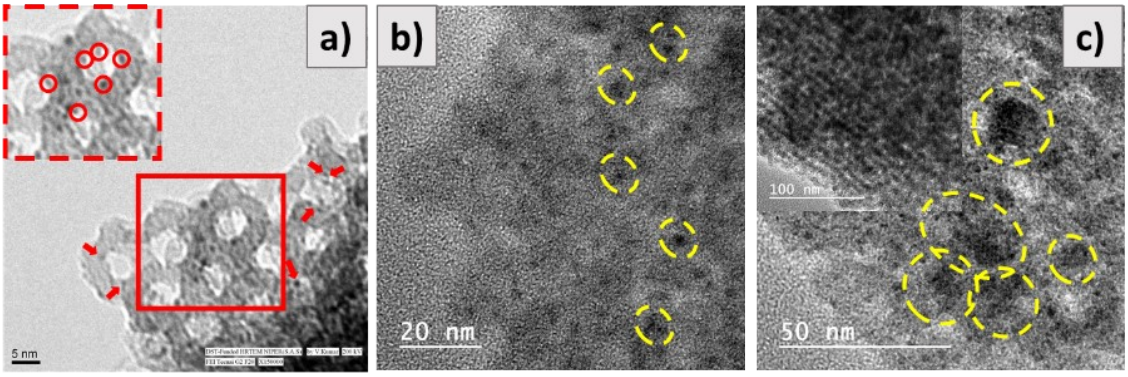

Figure S7. HRTEM images of Rh/SiO_2 with different particle sizes, where a) 0.8-1 nm, b) 3-4 nm, and c) > 10 nm

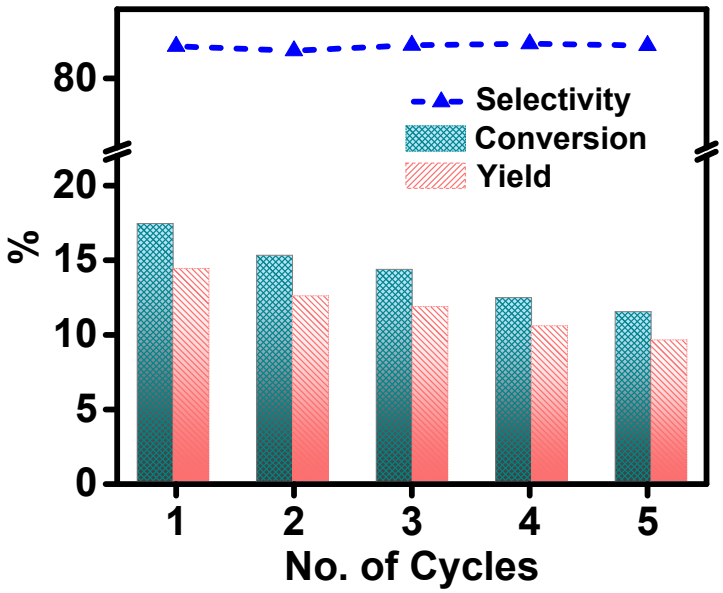

Figure S8. Recyclability tests of Rh/SiO_2 catalyst towards direct addition of ethylene to piperidine.

Table S2. Correlation between particle size of Rh_2O_3 (Rh/SiO_2) and conversion of piperidine[a]

Particle Size	Conversion of Piperidine (%)
0.8-1	14.5-15.6
3-4	6.8-7.5
>10	~3.5

[a]Reaction Conditions: Pressure of ethylene (12 Bar), Reaction temperature = 160 °C, Amount of piperidine = 0.0294 mol, amount of Rh/SiO_2 = 30 mg (8.163×10^{-3} mmol of Rh), Reaction time = 24 hours.

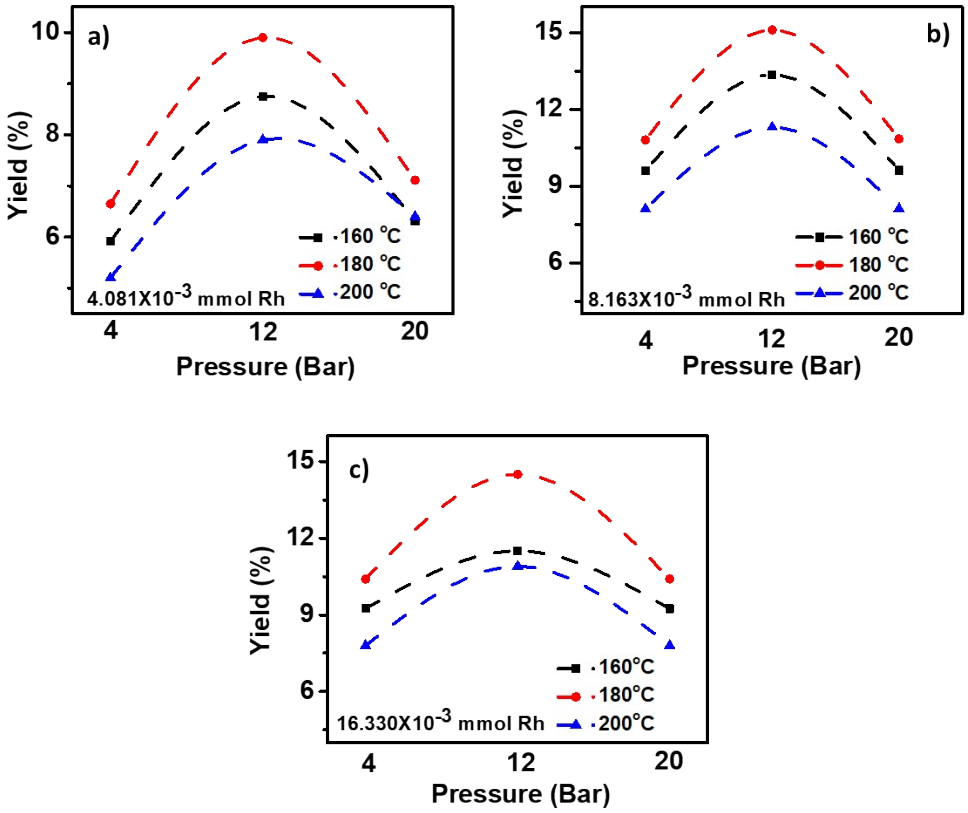

Figure S9. Effect on yield of N-ethyl piperidine on varying temperature and pressure when Rh concentration is a) 4.081×10^{-3} mmol, b) 8.163×10^{-3} mmol, and c)16.330×10^{-3} mmol.

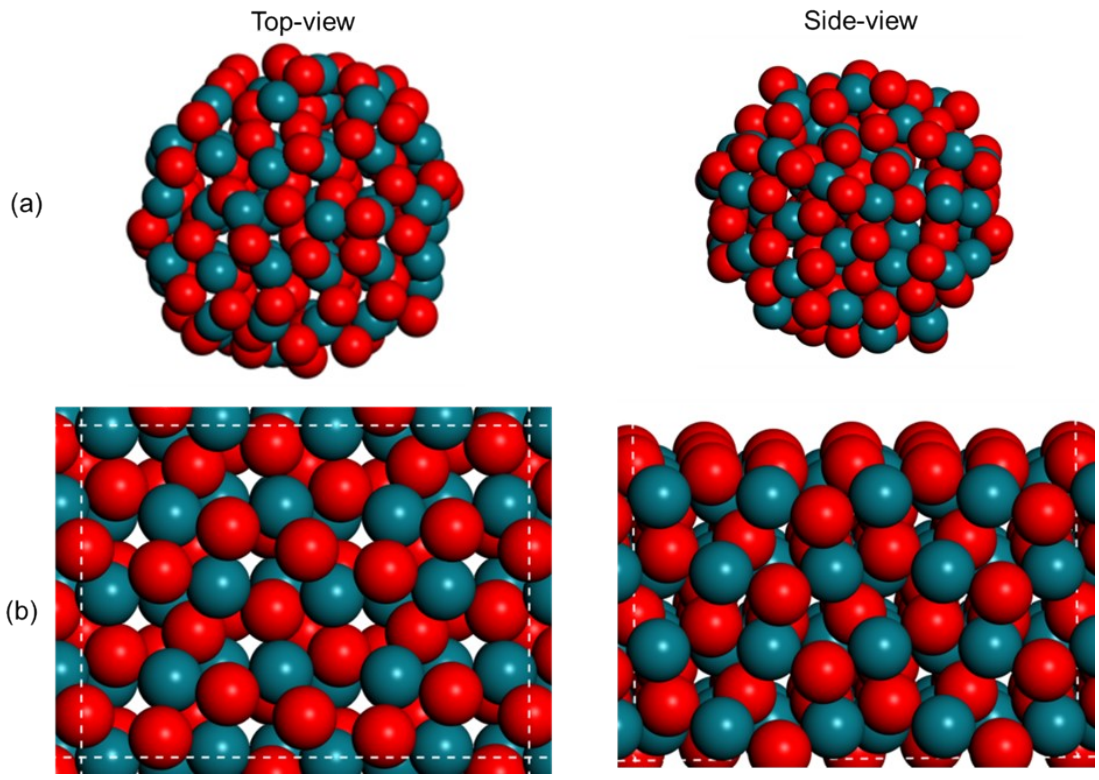

Figure S10. DFT optimized geometries of (a) $Rh_{80}O_{120}$ nanocluster and (b) $Rh_2O_3(100)$ surface.

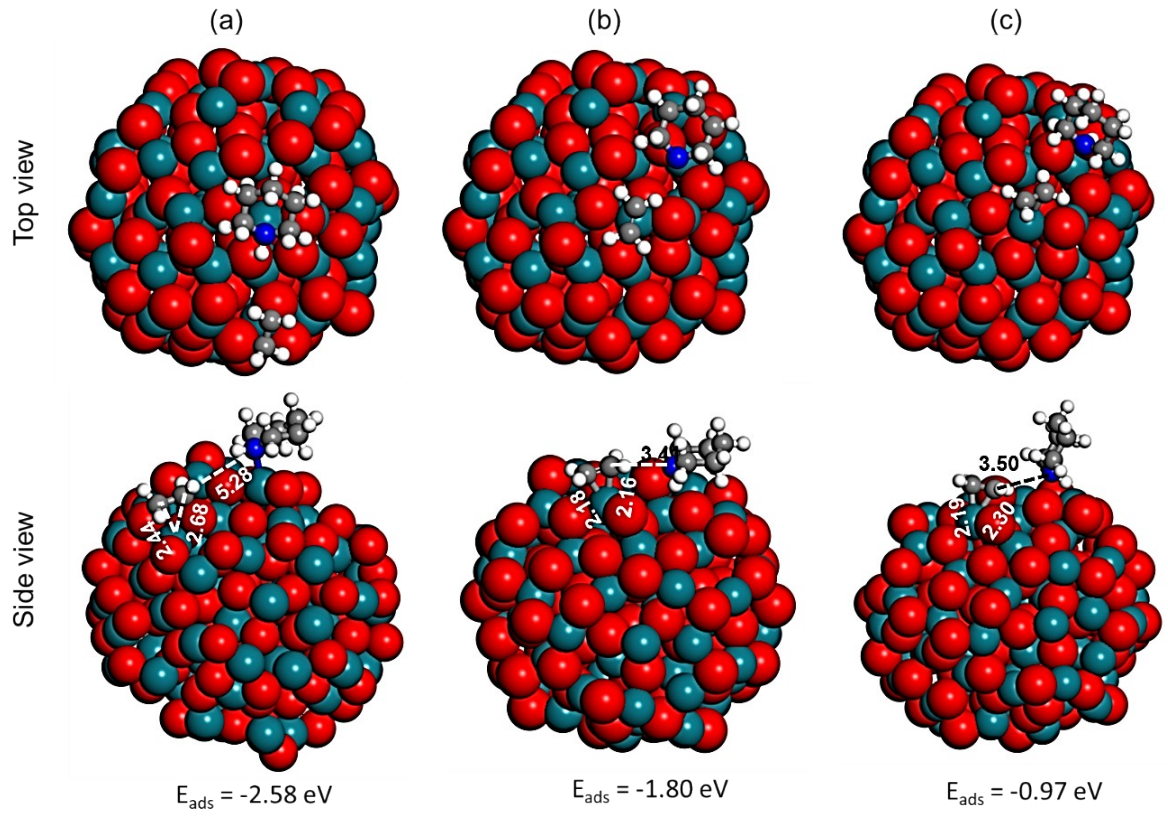

Figure S11. DFT optimized geometries of coadsorbed piperidine ($C_5H_{10}NH$) + ethylene (C_2H_4); over $Rh_{80}O_{120}$ nanocluster, Colour code: Rh (green), O (red), C (black), N (blue), H (white).

References

[1] a) A. Poswal, A. Agrawal, A. Yadav, C. Nayak, S. Basu, S. Kane, C. Garg, D. Bhattachryya, S. Jha, N. Sahoo, in *AIP Conference Proceedings, Vol. 1591*, American Institute of Physics, **2014**, pp. 649-651; b) S. Basu, C. Nayak, A. Yadav, A. Agrawal, A. Poswal, D. Bhattacharyya, S. Jha, N. Sahoo, in *Journal of Physics: Conference Series, Vol. 493*, IOP Publishing, **2014**, p. 012032.

[2] M. Newville, B. Ravel, D. Haskel, J. Rehr, E. Stern, Y. Yacoby, *Physica B: Condensed Matter* **1995**, *208*, 154-156.

[3] G. Kresse, J. Furthmüller, *Computational materials science* **1996**, *6*, 15-50.

[4] B. Hammer, L. B. Hansen, J. K. Nørskov, *Physical review B* **1999**, *59*, 7413.

[5] D. Vanderbilt, *Physical review B* **1990**, *41*, 7892.

[6] S. Grimme, S. Ehrlich, L. Goerigk, *Journal of computational chemistry* **2011**, *32*, 1456-1465.

[7] H. J. Monkhorst, J. D. Pack, *Physical review B* **1976**, *13*, 5188.

[8] D. Sheppard, R. Terrell, G. Henkelman, *The Journal of chemical physics* **2008**, *128*, 134106.

[9] G. Henkelman, B. P. Uberuaga, H. Jónsson, *The Journal of chemical physics* **2000**, *113*, 9901-9904.